Cooperativity and Spatial Correlations near the Glass Transition: Computer Simulation Results for Hard Spheres and Discs

B. Doliwa[*] and A. Heuer

Max-Planck-Institut für Polymerforschung, Postfach 3148
D-55021 Mainz, Germany

Abstract

We examine the dynamics of hard spheres and discs at high packing fractions in two and three dimensions, modeling the simplest systems exhibiting a glass transition. As it is well known, cooperativity and dynamic heterogeneity arise as central features when approaching the glass transition from the liquid phase, so an understanding of their underlying physics is of great interest. Cooperativity implies a reduction of the effective degrees of freedom, and we demonstrate a simple way of quantification in terms of the strength and the length scale of dynamic correlations among different particles. These correlations are obtained for different dynamical quantities $X_i(t)$ that are constructed from single-particle displacements during some observation time t. Of particular interest is the dependence on t. Interestingly, for appropriately chosen $X_i(t)$ we obtain finite cooperativity in the limit $t \to \infty$.

---

[*]email: doliwa@mpip-mainz.mpg.de

The remarkable features of glass-forming liquids, so is agreed to presently, can widely be attributed to collective phenomena. We know that they become more and more important if we approach the glass-transition point. It is a great challenge to understand collective phenomena because we expect them to be a kind of universal origin of glassy behavior.

The goal of this paper is to introduce a way of quantifying the degree of cooperativity by exploiting the correlations of two-time, single-particle quantities. This will be done for two- and three-dimensional systems thus revealing their very similar behavior. Naturally, these correlations have a spatial aspect, which shall be examined in detail. In principle, the idea is not new, because a considerable amount of work has recently been done on this subject [1, 2, 3, 4]. Even an experimental determination of dynamical length scales has become possible through multi-dimensional NMR [5, 6]. Particularly interesting, the theory of spin glasses makes predictions about the behavior of dynamic susceptibilities and - connected to it - dynamical length scales, when approaching the glass transition [7]. Summing spatial correlations, the susceptibility shows a divergence for the analyzed spin model near the mode-coupling critical temperature T_c^+. There is some evidence, that this divergence is present in structural glasses, too [8, 9].

Up to now, the discussion of dynamical length scales has mainly been focussed on the mobility of particles, but not on their direction of motion. Various versions of spatial correlators are in use, e.g. $\langle \mu(0,t)\mu(R,t)\rangle$, where $\mu_i(t)$ represents the length of the total displacement during $[0,t]$, i.e. the mobility, see [8]. As another example, one attributes to $\mu_i(t)$ the value of one, if particle i is slow, and zero else [9], see section 2. We will demonstrate, however, that the directional aspect of motion is crucial for interparticle correlations, resulting, e.g., in a much stronger density dependence of dynamical length scales.

From correlators of the above type, we can obtain the spatial extent as well as the overall, or mean, degree of cooperativity in the system's motion. In literature, one uses the detour via Fourier space and the fitting of Orstein-Zernike functions, to determine dynamical length scales. Throughout the present work, however, we will stay in real space, which will ease the interpretation of our data.

We will present a treatment of the overall cooperativity, which, in contrast to existing work, makes possible a pictorial understanding of our results in terms of a reduction of degrees of free-

dom. An important point is the time scale t defining the dynamical measurements. We hope to demonstrate, first, that dynamical length scales strongly depend on t, and, second, that $t = \tau_\alpha$ is not a sensible choice. Furthermore we show that the reduction of the degrees of freedom is directly related to the Haven ratio, well known to characterize cooperativity effects for the ion dynamics in ion conductors [10].

The organization of the paper is as follows. Section 1 gives the details of the performed simulations and introduces the main dynamical features via common single-particle quantities. Section 2 formulates our approach to quantify the system's overall cooperativity, which is well-known to be the integral of spatial correlations. The latter are treated in section 3, obtaining their strength and length scale. We conclude by a discussion of our results in section 4.

1 Simulation details

It is the advantage of a hard-sphere (HS) system for computer experiments, that the pair potential

$$ V_{ij}(r_{ij}) = \left\{ \begin{array}{ccc} \infty & : & r_{ij} < R_i + R_j \\ 0 & : & \text{otherwise} \end{array} \right. $$

forbids certain regions of configurational space, so that Monte Carlo steps are simply denied when particle overlaps occur. These computer-friendly 'yes/no' decisions make a Monte Carlo implementation of HS dynamics very efficient. The volume fraction

$$ \varphi_{3d} \equiv \frac{1}{V} \sum \frac{4}{3}\pi R_i^3, \text{ for } d=3 $$

or

$$ \varphi_{2d} \equiv \frac{1}{V} \sum \pi R_i^2, \text{ for } d=2 $$

takes the role of temperature, which is not a relevant control parameter here.

An important input parameter is the distribution of particle sizes R_i, i.e. the polydispersity. It determines to a large extent, how amorphous the system is. For example, a bimodal mixture of spheres can be used to prevent crystallization. In this work, we use a continuous, gaussian distribution of width σ_P and mean radius $\langle R_i \rangle = 1$, the latter serving as the unit of length. Particles of $|R_i - 1| > 3\sigma_P$ were not used, because they would slow down the simulations very much. Former experiments show, that for 3d systems, $\sigma_P = 10\%$ is enough to obtain a stable amorphous state, i.e. lacking long-range order [11]. In the

two-dimensional case (discs), we will work with $\sigma_P = 25\%$.

Although a HS system seems rather artificial at first sight, there is great interest in its properties, from both the theoretical and the experimental side. That, on the one hand, is due to the unbeatable simplicity, and on the other hand to the fact that HS are well represented by colloids in real life. Microscopically, colloidal particles perform free diffusion in their solvent, which is one of the reasons why we have chosen a Monte Carlo algorithm to generate the dynamics. Rather than integrating Newton's $F = ma$, we propagate the system according to the Langevin equation

$$\zeta \dot{\mathbf{r}}_i = -\boldsymbol{\partial}_i V(\mathbf{r}_1, ...\mathbf{r}_N) + \boldsymbol{\eta}_i, \qquad (1)$$

where white noises $\boldsymbol{\eta}_i(t)$ are directly coupled to the particles' *positions*. For very short waiting times t, there will hardly be any collision, so the potential term in Equ.(1) can be neglected. The result is a free diffusion for $t \to 0$, i.e. $\langle r^2(t) \rangle \approx 2dD_0 t$, where $d \in \{2, 3\}$ denotes the number of dimensions. All particles have equal masses, and their microscopic diffusion constants D_0 will be the same. Although this kind of dynamics is convenient for simulations, the approach via Newton's equations (molecular dynamics) would lead to quite similar results. Naturally, the trivial short-time motion would be completely different from the Monte Carlo case, but the relevant information for longer times is expected to be insensitive to the microscopic dynamics. Recently, this has been demonstrated for a Lennard-Jones type system [12].

In a Monte Carlo step, we randomly choose a particle and try to displace it a random amount $d\mathbf{x}$, whose distribution has the width λ. Thus, λ is the typical step length. We must take it as small as possible, because only in the limit $\lambda \to 0$, we are sure to integrate Equ.(1) correctly. On the other hand, a too small λ will reduce our simulation efficiency extremely, because upon halving λ, we need four times as many steps to cover the same distance. As a compromise, we try to achieve an acceptance rate of 50 percent, i.e. half of the displacements should result in valid moves, that is, producing no particle overlaps. Dependent on the packing fraction, this yield values from $\lambda = 0.02$ to $\lambda = 0.05$, i.e. a few percent of the mean particle radius. Comparisons to simulation runs with much smaller step sizes showed this choice to be sensible because no deviations arose, except for a trivial shift of time axis.

In the simulations analyzed in this paper, we used relatively large systems in order to prevent major finite size effects. To be more specific, we have $N =$ 8756, 8960, 9201 and 9320 for the two-dimensional systems at $\varphi_{2d} =$ 0.73, 0.75, 0.77 and 0.78, which correspond to a box length of a hundred mean particle diameters. In the three-dimensional case, we used $N =$ 15422 and 16307 particles filling a volume $(50R_0)^3$, i.e. 25 mean particle diameters in each direction. The corresponding volume fractions are $\varphi_{3d} =$ 0.53 and 0.56.

To get a first impression of the system's dynamics, it is most simple to calculate two-time, one-particle quantities. They show the same strong dependence on packing fraction as macroscopic transport quantities, like viscosity, when approaching the glass transition. The
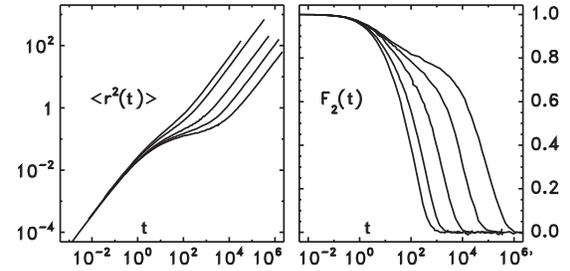

Fig. 1: One-particle, two-time quantities for the 3d packing fractions $\varphi_{3d} = 50\%, 53\%, 56\%, 57.3\%$ and 58%, from left to right. The system sizes are $N \approx 1000$. (a) the mean squared displacement $\langle r^2(t) \rangle$, and (b) the incoherent scattering function $F_2(\mathbf{k}_{\max}, t)$.

mean squared displacement

$$\langle r^2(t) \rangle \equiv \left\langle \frac{1}{N} \sum_i \left(\mathbf{r}_i(t) - \mathbf{r}_i(0) \right)^2 \right\rangle$$

and the incoherent part of the scattering function at a given wave vector $\mathbf{k}$,

$$F_2(\mathbf{k}, t) = \left\langle \frac{1}{N} \sum_i e^{i\mathbf{k}(\mathbf{r}_i(t) - \mathbf{r}_i(0))} \right\rangle$$

are the most common examples (see Fig. 1). The data shown in the figure above have been calculated in an earlier work, using small 3d systems of $N \approx 1000$ particles. In the following, this data will not be used anymore. Interestingly, the one-particle quantities in Fig. 1 differ little from their counterparts in the large N systems, i.e. for the analyzed packing fractions $\varphi_{3d} = 0.53$ and 0.56. The relaxation times τ_α, for

instance, agree within 20% at $\varphi = 0.56$. Many-particle correlations, in contrast, have turned out to be very sensitive to system size, see below. Simulation runs for $\varphi_{3d} > 0.56$ with numbers of particles $N > 10000$ are not available at the moment, but the densities $\varphi_{3d} = 0.53$ and 0.56 seem to produce all the interesting features of a cold glass-forming liquid.

We want to emphasize at this point that the one-particle quantities for the two-dimensional case look very similar to Fig. 1, i.e. we find anomalous diffusion, as expressed by the slope of $\langle r^2(t) \rangle$, and a plateau in the scattering function F_2, when going to high densities (not shown here). We can extract from $\langle r^2(t) \rangle$ the ratio $\frac{D}{D_0}$ of the long- and short-time diffusion constants. It describes the slowing down of the particles' long-distance motions upon increasing φ. The structural relaxation time τ_α is calcu-
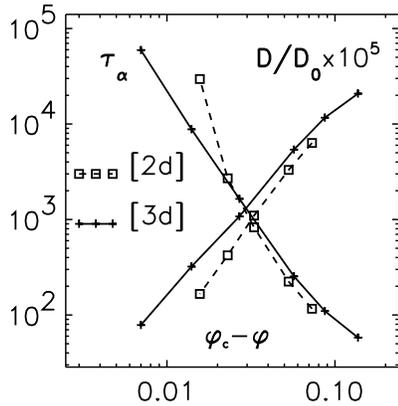
Fig. 2: Relaxation times $\tau_\alpha(\varphi)$ and diffusion constants $\frac{D}{D_0}(\varphi)$ for 2d and 3d systems. The critical values φ_c are determined by a MCT fit of the diffusion constant, i.e. $\frac{D}{D_0} \sim (\varphi_c - \varphi)^{-\gamma}$. The results are $\varphi_{c,3d} = 58.7\%$ and $\varphi_{c,2d} = 80.3\%$.

lated according to the condition $F_2(\mathbf{k}, \tau_\alpha) = \frac{1}{e}$, where the wave vector $\mathbf{k} = \mathbf{k}_{max}$ corresponds to the next-neighbor distance. The increasing τ_α and the decreasing $\frac{D}{D_0}$ indicate a great change of the dynamics when approaching a critical value of $\varphi_{c,3d} = 58.7\%$ in three and $\varphi_{c,2d} = 80.3\%$ in two dimensions, see Fig. 2. We obtained φ_c by a fit of $\frac{D}{D_0}(\varphi)$ to a power law $\frac{D}{D_0}(\varphi) \sim (\varphi_c - \varphi)^{-\gamma}$ as predicted by mode coupling theory [13]. However, the exact value of φ_c should not be over-interpreted because fits to a Vogel-Fulcher behavior $\frac{D}{D_0}(\varphi) \sim \exp(-\frac{C}{\varphi_c - \varphi})$ work equally well,

resulting in $\varphi_{VF,3d} = 0.612$ and $\varphi_{VF,2d} = 0.815$.

In the case of a HS system, the reason for the reduction of mobility at high φ is quite easy to understand. The particles are tightly surrounded by the so called *cages* of next neighbors which to a large degree restrict their motions. On average, a particle feels a back-dragging force, which prevents its cage from being destroyed, [14, 15]. If we define $\mathbf{x}_i^{(m)}(\epsilon) \equiv \mathbf{r}_i(t = m\epsilon) - \mathbf{r}_i(t = m\epsilon - \epsilon)$ as the subsequent displacements of a tagged particle, the back-dragging force results in a negative value of the correlation $\langle \mathbf{x}^{(1)} \mathbf{x}^{(m)} \rangle$. With the Green-Kubo relation

$$ D = D_0 + \frac{1}{\epsilon d} \lim_{M \to \infty} \sum_{m=2}^{M} \langle \mathbf{x}^{(1)} \mathbf{x}^{(m)} \rangle, $$

this immediately leads us to the conclusion that the so called cage effect is responsible for the slowing down of the motion, as expressed by $D < D_0$.

On a longer time scale, the particles finally succeed in leaving their cages. Naturally, this can only occur if the neighbors rearrange in a collective way.

2 Cooperative Effects

Figure 3 suggests the fact that a liquid near its glass transition possesses beautiful and highly non-trivial dynamics, see also [16, 17]. We
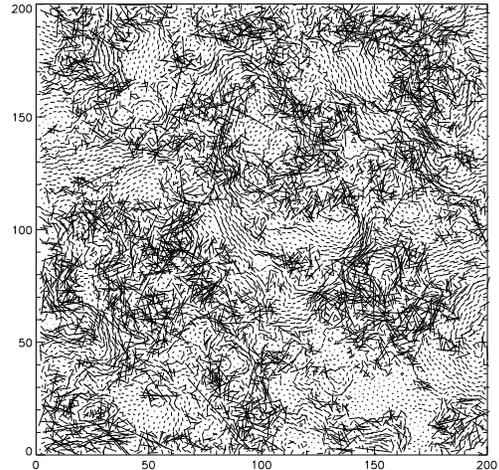
Fig. 3: Particle motions $\mathbf{r}_i(t+50\tau_\alpha) - \mathbf{r}_i(t)$ during a time $50\tau_\alpha$. The density is $\varphi = 0.78$ in a 2d-system.

recognize regions of totally different behavior, some of which show very crowded and uncooperative motions, while others seem to act *as one*

resulting in collective flows. The mobility obviously varies between different areas, which is commonly referred to as *dynamic heterogeneity*. How can we quantify the degree of cooperativity in our system? It is possible to do this by comparing the fluctuation of a one-particle dynamic quantity X_i with its many-particle equivalent $\sum_i X_i$. For simplicity, let $\langle X_i \rangle = 0$, which implies $\langle \sum X_i \rangle = 0$. We can think of X_i to be the displacement vector $X_i = \mathbf{v}_i \equiv \mathbf{r}_i(t + t') - \mathbf{r}_i(t)$ or its relative length $X_i = \delta v_i \equiv v_i - \langle v_i \rangle$, where $v_i \equiv |\mathbf{v}_i|$. The direction of motion $\mathbf{n}_i \equiv \mathbf{v}_i v_i^{-1}$ is a sensible choice for X_i, too. In the case where interparticle correlations are lacking, the width of the distribution of X will be

$$\text{Var}\left[\sum X_i\right] = \sum \text{Var}\left[X_i\right].$$

Correlations, however, will increase $\text{Var}\left[\sum X_i\right]$ while anti-correlations will do the opposite. From Fig. 3, it is reasonable to expect *correlations*, and we define

$$N_X^{\text{coop}} \equiv \frac{\text{Var}\left[\sum X_i\right]}{\sum \text{Var}\left[X_i\right]} = 1 + \frac{\sum_{i \neq j}\langle X_i X_j \rangle}{\sum \langle X_i^2 \rangle}. \quad (2)$$

If our expectation is right, then N_X^{coop} will be larger than one.

We now claim that N_X^{coop} measures the total reduction of degrees of freedom caused by correlations. In the simple case of uncorrelated motion ($\langle X_i X_j \rangle = 0$), we obtain $N_X^{\text{coop}} = 1$, whereas the other extreme of totally correlated motion ($X_i \equiv X_j$) results in $N_X^{\text{coop}} = N$. If, more generally we have M identical variables X_i in each of L independent groups, $N = ML$, we obtain

$$N_X^{\text{coop}} = 1 + \frac{1}{\sum \langle X_i^2 \rangle} \sum_{i=1}^{N} \sum_{j=1}^{M-1} \langle X_i^2 \rangle = M.$$

These examples show that N_X^{coop} is indeed a reasonable quantitative measure for the degree of cooperativity. In real life, correlations will not be perfect, i.e. a hundred percent, and their strengths and spatial extensions will vary throughout the system. Hence, we should expect N_X^{coop} to be an average or effective reduction factor for the degrees of freedom.

It is important to note that $N_X^{\text{coop}} = N_X^{\text{coop}}(t)$ because the dynamic quantities $X_i = X_i(t)$ are dependent on the time scale necessary for their definition. The calculation of N_X^{coop} turns out to be quite unconvenient. From one configuration, we only get one data point for the term $\sum_i X_i$ in the numerator, i.e. N_X^{coop} is not self-averaging. Thus, the simulation run has to be very long to

aquire enough points for the calculation of the variance. A way around this obstacle is not to sum over the whole system, but only over local subsystems of n particles. This should improve statistics. In practice, at a given n, we randomly choose a central particle and add the closest $(n-1)$ neighbors using them as a subsystem. Repeating this procedure for a small number of other central particles, we get some more subsystems of size n.
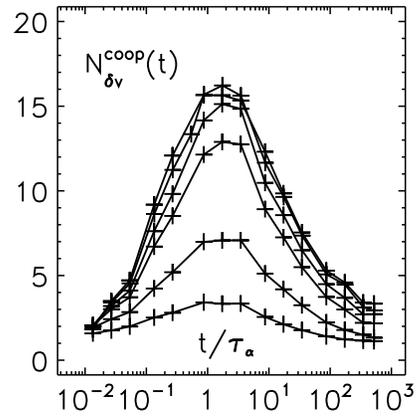

Fig. 4: $N_{\delta v}^{\text{coop}}(t)$ at density $\varphi_{3d} = 0.56$, for different numbers n of particles, that are summed over in $\sum_i X_i$. From bottom to top: $n = 20, 100, 500, 1000, 2000,$ and 4000. Time is normalized to τ_α.

Naturally, a too small n will modify our results because we throw away some longer-ranged correlations, which can be important. An illustration for that is given in Fig. 4, where $N_{\delta v}^{\text{coop}}$ belonging to $X_i = \delta v_i \equiv v_i - \langle v_i \rangle$ is plotted for different n at density $\varphi_{3d} = 0.56$. We clearly see that it is necessary to take as many as $n > 1000$ particles because a major change can be found when decreasing n from there. Interestingly, we obtained for a small system of $N = 1066$, $\varphi_{3d} = 0.56$ only a maximum $N_{\delta v}^{\text{coop}}$ of nine when using $n = 1066$ for its calculation (data not shown). This is half of the value of $N_{\delta v}^{\text{coop}}$ at $N = 16307$, $n = 1000$, thus proving large finite size effects in many-particle correlations for the small system. Being conscious of this problem is especially important if one needs trustable numerical values for N_X^{coop}, e.g. for determining the exponent of divergence when cooling towards the glass transition, as is done in [9]. How is it possible that $N_{\delta v}^{\text{coop}} < 20$ in the case $\varphi_{3d} = 0.56$ although the finite-size effects of a too small subsystem n can be sensed even

up to $n = 1000$? The reason is that particles are only partially correlated, which will become clear in the next section where we demonstrate the decay of correlations with interparticle distance. Additionally, regions of fast particles are extended, non-compact objects (Fig. 3), so that we have to sum over larger subsystems to include all their mobility correlations.

On the other hand, however, taking n as large as possible is not always the best thing to do. We can see the reason for this at the example $X = \mathbf{v}$ taking $n = N$, i.e. all particles of the system. Then, $\mathrm{Var}\left[\sum \mathbf{v}_i\right] = 0$ because the simulation conserves the center of mass, which means it sets $\sum \mathbf{v}_i$ to zero. Fortunately, our systems are large enough, enabling us to choose an optimum value of n just between these two size effects. For a more thorough discussion see Fig. 7 and the corresponding text below.

A word about error bars. The statistically uncertainty of simulation results is a consequence of the limited length T of the runs. If we assume the equivalence of ensemble and time average, a quantity A can be determined up to accuracy $\mathrm{Var}_T[A] \sim T^{-1}$ where the constant of proportionality is essentially the decay time of the autocorrelation function $\langle A(t)A(0)\rangle$. We calculate $\mathrm{Var}_T[A]$ by extrapolating its behavior for $T' < T$ to T, i.e. the average over the whole simulation run. This is done for $A \equiv N_X^{\mathrm{coop}}(t)$, only for few examples of t. The resulting errors $\delta N_X^{\mathrm{coop}} = \pm \left(\mathrm{Var}\left[N_X^{\mathrm{coop}}\right]\right)^{\frac{1}{2}}$ are given in the figure captions.

Figure 5 shows $N_X^{\mathrm{coop}} = N_{\delta v}^{\mathrm{coop}}$ for some densities φ in two and three dimensions. As a function of time, $N_{\delta v}^{\mathrm{coop}}$ starts at short times with the value of one because the individual brownian motions in the microscopic regime are uncorrelated. This is a trivial statement, so we do not have to demonstrate it for every density. For later times, $N_{\delta v}^{\mathrm{coop}}$ reaches a maximum which is strongly increasing with density. The following decay then takes some decades in time again. But as can be seen, a limiting value is hard to observe within simulation times, see below.

Now, the behavior of 2d and 3d systems seems to be quite similar, although the maximum values of $N_{\delta v}^{\mathrm{coop}}$ are larger in 2d. A small difference is the shift of the 2d maxima towards longer times. While in 3d they are found at approximately $2\tau_\alpha$, we find them in the 2d case at around $4\tau_\alpha$. This shift can be observed in other dynamical quantities as well. The simple reason lies in the different polydispersities $\sigma_{\mathrm{P}} = 0.1$ in three and $\sigma_{\mathrm{P}} = 0.25$ in two dimensions. In 2d, the small
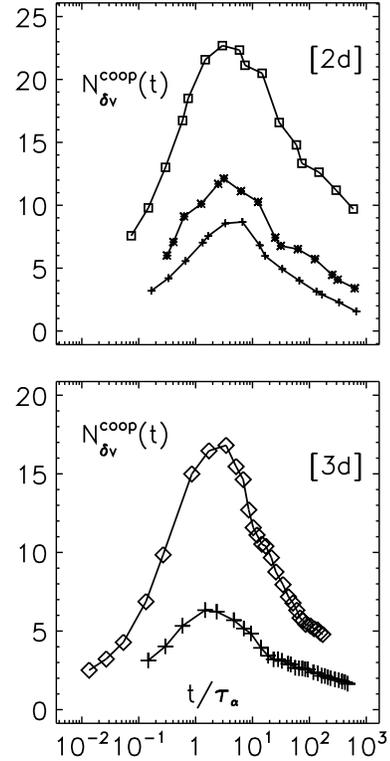

Fig. 5: [2d]:$N_{\delta v}^{\mathrm{coop}}(t)$ for $n = 2000$ at $\varphi_{2d} = 0.73, 0.75$ and 0.77 [3d]:The same for the 3d case, $\varphi_{3d} = 0.53$ and 0.56. The statistical error due to the finite simulation time is $\delta N_{\delta v}^{\mathrm{coop}}(20\tau_\alpha) = \pm 0.5$ for $\varphi_{3d} = 0.56$. Again, time-normalization by τ_α.

and - on average - fast particles cause $F_2(\mathbf{k}_{\mathrm{max}}, t)$ to decay more quickly in the beginning, so we measure a systematically smaller τ_α than in the 3d case. If we defined $F_2(\mathbf{k}_{\mathrm{max}}, \tau_\alpha) = 0.01$ instead of requiring $F_2(\mathbf{k}_{\mathrm{max}}, \tau_\alpha) = \frac{1}{e}$, this discrepancy would vanish.

It is important to compare these results with N_X^{coop} determined by the dynamical quantities $X = \mathbf{v}$ or $X = \mathbf{n}$ as mentioned above. For the interpretation of values of N_X^{coop}, this is essential, because different sensible quantities X should not produce totally different values of N_X^{coop}. Figure 6 shows the case $X = \mathbf{v}$ for 2d and 3d, and $X = \mathbf{n}$ for 3d. Firstly, $N_{\mathbf{v}}^{\mathrm{coop}}$ and $N_{\mathbf{n}}^{\mathrm{coop}}$ clearly display their long-time limits, which are equal and different from one. Secondly, $N_{\mathbf{n}}^{\mathrm{coop}}$ still develops a maximum around $t = \tau_\alpha$, while $N_{\mathbf{v}}^{\mathrm{coop}}$ is a monotonously increasing function. Table 1 summarizes the main results about N_X^{coop}. We can compare the maximum values of N_X^{coop} for equivalent densities (e.g. equivalent in the sense of
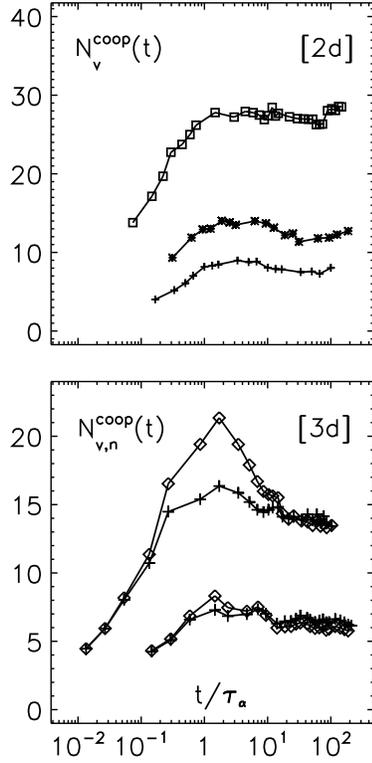
Fig. 6: [2d]: $N_{\mathbf{v}}^{\text{coop}}(t)$ for $n = 2000$ at $\varphi_{2d} = 0.73, 0.75$ and 0.77. [3d]: The same for the 3d case, $\varphi_{3d} = 0.53$ and 0.56, $n = 2000$ (+). Additionally, we see $N_{\mathbf{n}}^{\text{coop}}(t)$ ($\diamond$). The statistical error is $\delta N_{\mathbf{v}}^{\text{coop}}(10\tau_\alpha) = \pm 0.5$ at $\varphi_{3d} = 0.56$, and $\delta N_{\mathbf{v}}^{\text{coop}}(50\tau_\alpha) = \pm 1.3$ at $\varphi_{2d} = 0.77$, for example. Time is normalized by τ_α .

Table 1:

φ_{2d}	$\ln \frac{D_0}{D}$	$N_{\delta v,\text{max}}^{\text{coop}}$	$N_{\mathbf{v},\infty}^{\text{coop}}$
0.73	2.76	9	8 (10)
0.75	3.41	12	13 (17)
0.77	4.51	23	28 (35)

φ_{3d}	$\ln \frac{D_0}{D}$	$N_{\delta v,\text{max}}^{\text{coop}}$	$N_{\mathbf{v},\infty}^{\text{coop}}$	$N_{\mathbf{n},\text{max}}^{\text{coop}}$
0.53	2.92	6.5	6 (7)	8
0.56	4.53	17	14 (16.5)	21

equal $\frac{D}{D_0}$) and find a somewhat higher cooperativity in 2d. The absolute values of N_X^{coop} for the different X agree to a reasonable extent, so that we are indeed allowed to interpret them in the sense of a reduction factor for the degrees of freedom.

Let us now turn to the limiting value $N_{\mathbf{v},\infty}^{\text{coop}}$.

Although we find a random diffusion for every particle on a time scale $t \gg \tau_\alpha$ as expressed by the diffusion law $\langle r^2(t) \rangle \sim Dt$, we should generally not expect N_X^{coop} to be one because the interparticle correlations from shorter times are still accounted for in this quantity. This can clearly be seen in the following way: We decompose the displacement $\mathbf{v}_i$ for $t \gg \tau_\alpha$ into M pieces, each of them corresponding to a time step $\epsilon = \frac{t}{M}$, i.e.

$$\mathbf{v}_i = \sum_{m=1}^{M} \boldsymbol{\Delta}_i^m,$$

for particle i. For simplicity, let us say that interparticle correlations are neglible for different time intervals, i.e. $\langle \boldsymbol{\Delta}_i^m \boldsymbol{\Delta}_j^{m'} \rangle = 0$ if $m \neq m'$. In this case, we obtain

$$N_{\mathbf{v}}^{\text{coop}}(t) = 1 + \frac{M \sum_{ij} \langle \boldsymbol{\Delta}_i^1 \boldsymbol{\Delta}_j^1 \rangle}{NM \sum_i \langle (\boldsymbol{\Delta}_i^1)^2 \rangle},$$

where we exploited time translational invariance, i.e. having an equilibrium liquid. This quantity, however, does not depend on time $t = M\epsilon$ anymore, if ϵ is fixed. We thus get an idea how it is possible that correlations persist for $t \to \infty$.

Finally, other choices of X_i are possible, e.g. more exotic quantities like

$$X_i = w_i \equiv \begin{cases} 1 & : & \text{slow} \\ -1 & : & \text{fast} \\ 0 & : & \text{otherwise} \end{cases},$$

where the exact definition of *fast* and *slow* is of no importance as long as it is done in a sensible way. Such an analysis has been presented in [9] for a Lennard-Jones fluid using a 'dynamic susceptibility' χ_{ss} instead of N_X^{coop}. Its definition is quite similar to N_X^{coop}, measuring fluctuations of a many-particle, 'macroscopic' dynamic quantity $Q_{\text{ss}} = \sum w_i$:

$$\chi_{\text{ss}} = \frac{\beta V}{N^2} \left[\langle Q_{\text{ss}}^2 \rangle - \langle Q_{\text{ss}} \rangle^2 \right].$$

Unlike N_X^{coop}, a quantitative interpretation of the value of χ_{ss} is not obvious.

Let us return to the role of the size n of the subsystems that are used for the calculation of N_X^{coop}. As we said above, the subsystem should be large enough to include most of the long-ranged correlations of its particles, i.e. to reduce surface effects. On the other hand, $n = N$ leads to $N_{\mathbf{v}}^{\text{coop}} = 0$ because of the center-of-mass correction (cmc). It is evident that our results will be influenced by the cmc even if we use $n < N$,
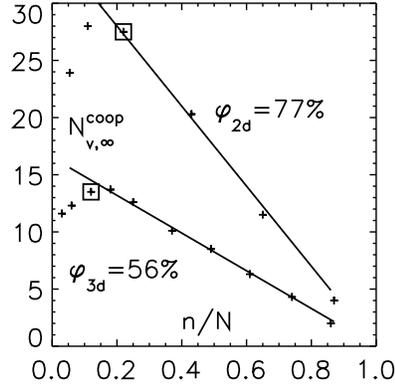
Fig. 7: The role of the subsystem size n in the calculation of $N_{\mathrm{v},\infty}^{\mathrm{coop}}$ (+), for the systems $\varphi_{2d} = 77\%$ ($N = 9201$) and $\varphi_{3d} = 55\%$ ($N = 16307$). The solid lines are fits of the form $N_{\mathrm{v,ren}}^{\mathrm{coop}}(1 - \frac{n}{N})$, where the parameter $N_{\mathrm{v,ren}}^{\mathrm{coop}} = 35$ and 16.5, in the 2d and 3d case, respectively. The $\square$ marks the choice $n = 2000$.

say $n = 0.9N$. Despite this fact, we need a cmc because the motion of the whole simulation box leads to unphysical results for $N_{\mathrm{x}}^{\mathrm{coop}}$. Interestingly, the center of mass performs a random walk with speed $\langle \mathbf{v}_{\mathrm{cm}}^2(t) \rangle = \frac{1}{N} 2dD_0 t$, independent of the packing fraction, which is the consequence of $actio = reactio$ in a stochastic sense. Now, the subtle point is that the cm motion consists of two contributions, firstly the random displacement $\mathbf{U}$ of the simulation box as a whole which would vanish if we embedded the simulation box in macroscopic system. Secondly, the random rearrangements $\mathbf{w}_i$ of particles in our system that produce a contribution to the cm motion even if we forbid an overall drift of the box. Obviously, we should keep the second and discard the first contribution because the latter is an artefact of the limited system size. A cmc, however, will remove both. In the following, we estimate the resulting error in the calculation of $N_{\mathrm{v}}^{\mathrm{coop}}$. The uncorrected displacement of particle i is $\mathbf{v}_i = \mathbf{w}_i + \mathbf{U}$, so that the cm motion becomes $\mathbf{v}_{\mathrm{cm}} = \frac{1}{N} \sum_{k=1}^N \mathbf{w}_k + \mathbf{U}$, where the first term does generally not vanish. Calculating the numerator of $N_{\mathrm{v}}^{\mathrm{coop}}$ in Equ.(2), we obtain

$$\sum_{ij=1}^n \langle (\mathbf{v}_i - \mathbf{v}_{\mathrm{cm}})(\mathbf{v}_j - \mathbf{v}_{\mathrm{cm}}) \rangle$$

$$= \sum_{ij=1}^n \left(\langle \mathbf{w}_i \mathbf{w}_j \rangle + \frac{1}{N^2} \sum_{kl=1}^N \langle \mathbf{w}_k \mathbf{w}_l \rangle \right.$$

$$\left. - \frac{2}{N} \sum_{k=1}^N \langle \mathbf{w}_i \mathbf{w}_k \rangle \right)$$

$$= \sum_{ij=1}^n \langle \mathbf{w}_i \mathbf{w}_j \rangle \left(1 - \frac{n}{N} \right),$$

where, in the final step, correlations between the $\frac{N}{n}$ different subsystems have been neglected. Thus,

$$N_{\mathrm{v}}^{\mathrm{coop}} = N_{\mathrm{v,ren}}^{\mathrm{coop}} \left(1 - \frac{n}{N} \right) \tag{3}$$

is the result, which is too small by a factor of $(1 - \frac{n}{N})$. As is demonstrated in Fig. 7 for the value of $N_{\mathrm{v}}^{\mathrm{coop}}(\infty)$, this behavior can indeed be observed in our simulations. The renormalized value of cooperativity, $N_{\mathrm{v,ren}}^{\mathrm{coop}}$, comes out as a fit parameter to the form of Equ.(3), see table 1 in the brackets. Additionally, Fig. 7 tells us what choice of n is advisable because $\frac{n}{N}$ has to be in a region where the above fit works. If this is the case, the subsystem must have only small remaining correlations with the other $N - n$ particles because increasing n only reduces $N_{\mathrm{v}}^{\mathrm{coop}}$ by the 'trivial' factor of $(1 - \frac{n}{N})$. The choice $n = 2000$ is marked by $\square$ in Fig. 7.

In our case, at $\varphi_{2d} = 0.77$, we observe a maximum reduction of the total degrees of freedom by a factor of $N_{\mathrm{v,ren}}^{\mathrm{coop}} = 35$. This, however, is yet only a moderately high density ($\varphi_{c,2d} \approx 0.8$), so we should expect large collective effects at the glass transition.

Finally we mention an interesting relation between $N_{\mathrm{v},\infty}^{\mathrm{coop}}$ and the Haven ratio, relating the ratio of the self-diffusion constant and the conductivity in ionically conducting materials. Its zero-frequency limit $H(0)$ is given by

$$H(0) = \frac{\sum_i \int_0^\infty dt \langle \mathbf{v}_i(0)\mathbf{v}_i(t) \rangle}{\frac{1}{N} \sum_{i,j} \int_0^\infty dt \langle \mathbf{v}_i(0)\mathbf{v}_j(t) \rangle}. \tag{4}$$

Since for large times $\langle \mathbf{v}_i^2(t) \rangle = 2dDt = 2t \int_0^\infty dt \langle \mathbf{v}_i(0)\mathbf{v}_i(t) \rangle$ and correspondingly $\langle \mathbf{v}_i(t)\mathbf{v}_j(t) \rangle = 2t \int_0^\infty dt \langle \mathbf{v}_i(0)\mathbf{v}_j(t) \rangle$, it is obvious that

$$N_{\mathrm{v},\infty}^{\mathrm{coop}} = H(0)^{-1}. \tag{5}$$

Hence, as a side product we have obtained a quantitative interpretation of the inverse Haven ratio as the reduction of the effective degrees of freedom.

3   Spatial Correlations

The snapshot of the dynamics in 2d (Fig. 3) demonstrates that large spatial correlations are

present in our systems. In the following, we want to quantify them as a function of the timescale of dynamics.

As in the treatment of N_X^{coop}, a dynamical variable X_i should be given for each particle, again with the restriction $\langle X_i \rangle = 0$. A spatial correlator can then be defined by

$$\langle X(\mathbf{0})X(\mathbf{R})\rangle \equiv \left\langle \frac{1}{N}\sum_{ij} X_i X_j \delta\left(\mathbf{R}-(\mathbf{r}_i-\mathbf{r}_j)\right)\right\rangle. \tag{6}$$

Again, X_i denotes a dynamical quantity connected to the motion of particle i during the time interval $[t_0, t_0+t]$. Because of symmetry reasons, the positions $\mathbf{r}_i = \mathbf{r}_i(t_0+\frac{t}{2})$ are used. Averaging over the solid angle of $\mathbf{R}$, i.e.

$$\langle X(0)X(R)\rangle \equiv \frac{1}{4\pi R^2}\int \mathrm{d}\Omega \langle X(\mathbf{0})X(\mathbf{R})\rangle,$$

results in a loss of information because the direction of motion of particle i, for example, breaks the isotropy. Figure 8 explains this in
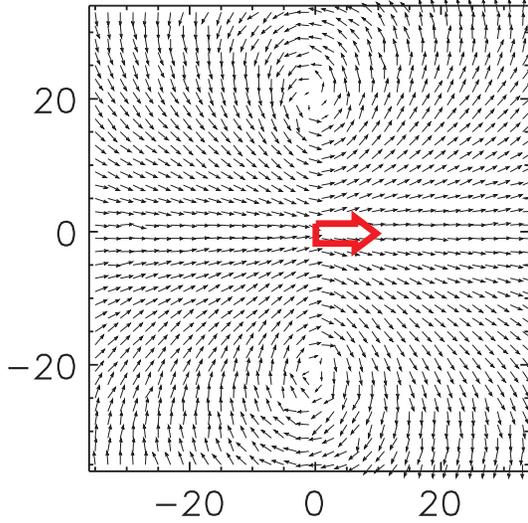

Fig. 8: Correlations of the direction of displacements, $X_i = \mathbf{n}_i$ at $\varphi = 77\%$, $t = 10\tau_\alpha$. The large arrow in the middle shows the direction of motion of the reference particle. For details, see text.

a pictorial way: particles "in front of" or "behind" the central one have a very long-ranged directional correlation, while perpendicular to the direction of motion, we observe a kind of back-flow behavior which is well-known from [18]. How has this plot been produced? First, we calculate all $X_i = \mathbf{n}_i$, i.e. the directions of displacements during a time interval $[t_0; t_0 + t]$.

We then choose particle i and turn the whole (2d) system so that X_i' points along the positive x-axis. Now, the directions X_j' are added to the average at the positions $\mathbf{r}_j'(t_0+\frac{t}{2})$. As result, we obtain the field $\langle X'(\mathbf{r}')\rangle$, which for large $||\mathbf{r}'||$ consists of very short vectors. Hence, for reasons of visualization, we plot the *normalized* version of $\langle X'(\mathbf{r}')\rangle$ in Fig. 8.

Being aware of the complicated behavior in Fig. 8, let us for the moment and for simplicity ignore the angle-dependence, and treat correlations only as a function of interparticle distance R. We define the dimensionless quantity

$$S_X(R,t) \equiv \frac{\langle X(0)X(R)\rangle}{\langle X^2(0)\rangle}, \tag{7}$$

where again its dependence on time-scale t should be kept in mind, just as in the case of N_X^{coop}. Possible choices are $X_i = \delta v_i$, $X_i = \mathbf{v}_i$ or $X_i = \mathbf{n}_i$, where $\mathbf{v}_i = \mathbf{r}_i(t) - \mathbf{r}_i(0)$, $\delta v_i = v_i - \langle v_i \rangle$ and $\mathbf{n}_i = \hat{\mathbf{v}}_i$. The functions $S_{\delta v}(R,t)$ and $S_{\mathbf{n}}(R,t)$ count correlations of both slow and fast particles because both sorts are weighted similarly. To be more precise, the slow particles are not suppressed as in the case of $S_{\mathbf{v}}(R,t)$.

Calculating $S_X(R,t)$, we encounter a problem that is related to the system size. If we want the system's center of mass to be constant, we have to correct the particles' motions. But this introduces an anti-correlation of two formerly uncorrelated particles. As a consequence, $S_X(R,t)$ will approach a negative value for large R, instead of zero. Without center-of-mass correction, we would measure a positive number in this limit because the center of mass performs a slow diffusive motion, see the previous section. For the present systems, these offsets were smaller than 0.002, which is a small fraction of the amplitude of correlation. Hence, their subtraction from $S_X(R,t)$ left the function nearly unchanged.

Figures 9 and 10 show $S_{\delta v}(R,t)$ for the 2d systems $\varphi_{2d} = 73\%$ and $\varphi_{2d} = 0.77$. Obviously, $S_{\delta v}(R,t)$ can be described by an exponential

$$S_{\delta v}(R,t) \approx A(t)\exp\left(-\frac{R}{\xi_{\delta v}(t)}\right) \tag{8}$$

to a good approximation, if $R > 5$. It is important to note that the amplitude $A(t)$ is not necessarily equal to one as suggested by the definition of $S_X(R,t)$ for $R \to 0$. In other words, the extrapolation of complicated inter-particle correlations to the one-particle quantity $S_X(R = 0, t)$ would be unphysical.
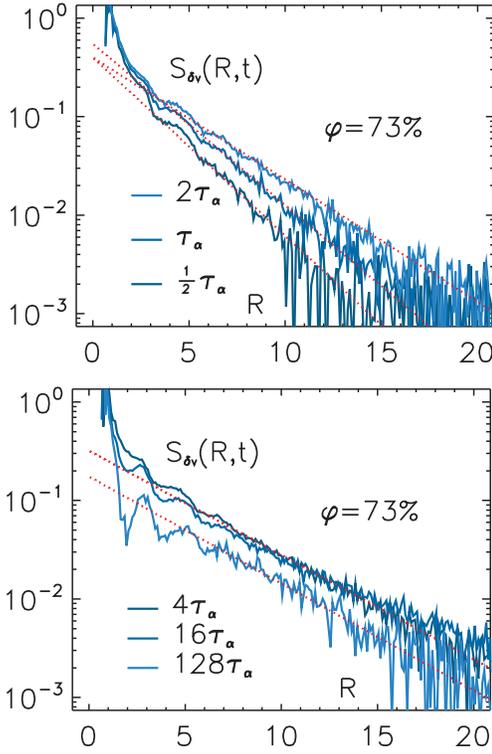
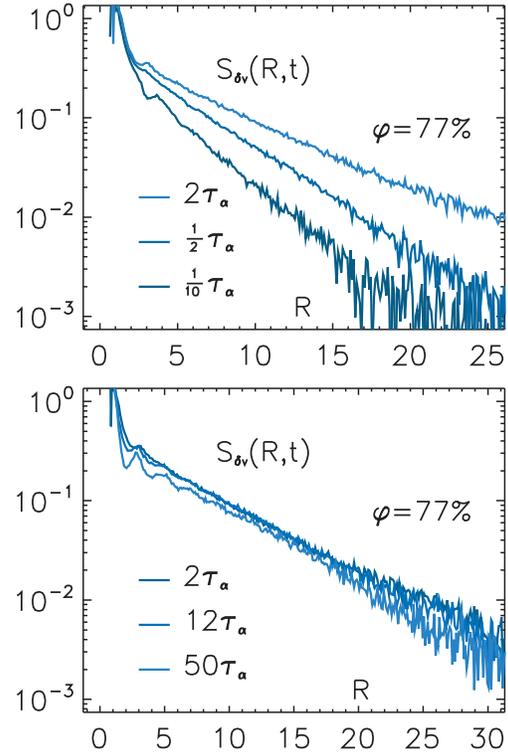Fig. 9: Spatial correlation $S_{\delta v}(R,t)$ at $\varphi_{2d} = 73\%$.

Fig. 10: Spatial correlation $S_{\delta v}(R,t)$ at $\varphi_{2d} = 77\%$.

We find large deviations from the exponential at distances $R < 5$. This can be understood qualitatively because certain information about the local packing is available. For instance, $R < 1$ can only occur for two very small particles (remember $\langle R_i \rangle = 1$) which on average are much faster than the others. Thus, $\langle \delta v(0) \delta v(R) \rangle$ will be quite large. The oscillations for $R < 6$ must have a similar reason, i.e. special local packings that are favorable or not for the value of $\langle \delta v(0) \delta v(R) \rangle$. We can imagine that for larger R, the possibilities of packing become so many that they average $S_X(R)$ to a structureless exponential. This is the case for the structure factor $g(R)$, too.

Figure 11 shows $S_{\delta v}(R,t)$ for the three-dimensional case. The situation is quite the same as in 2d, except for the long-range oscillations, especially of $S_{\delta v}(R, t = \tau_\alpha)$. They, too, indicate the existence of structures that are favourable for dynamical correlations. For 2d systems of smaller polydispersity $\sigma_P = 10\%$, which are not shown here, we find the same oscillations. In this case, they could be proved to result from local crystalline order, which occurs, if - by coincedence - many particles of approximately the same size come together. Al-

though the system is in an overall amorphous state, the small polydispersity makes local crystallites more probable, thus creating regions of low mobility. The oscillations for three dimensions, however, are not understood yet.

In any event, we can extract from $S_{\delta v}(R,t)$ the amplitude $A(t)$ and the correlation length $\xi_X(t)$ as a function of the dynamic time scale t. The simulation runs, by the way, have to be much longer than the maximum time scale shown because the functions $S_{\delta v}(R,t)$ are quite demanding with respect to statistics. For instance, distant particles, which are uncorrelated, have to average $\langle X(0)X(R) \rangle$ to zero. The statistics M enters by a factor of $\frac{1}{\sqrt{M}}$, so an improvement of the result has a high price. Additionally, the *dynamic heterogeneities*, as visualized in Fig. 3, are very long-lived [19], i.e. possess typical life-times of tens to hundreds of τ_α, dependent on φ. Thus, if we want to average over different dynamical situations, we need data for some hundreds of τ_α. Table 2 shows the lengths of our simulation runs in units of τ_α for the analyzed 2d and 3d packing fractions, respectively, including the system size N.

Let us turn to another dynamical quantity $X_i = \mathbf{n}_i$, the direction of displacement. As
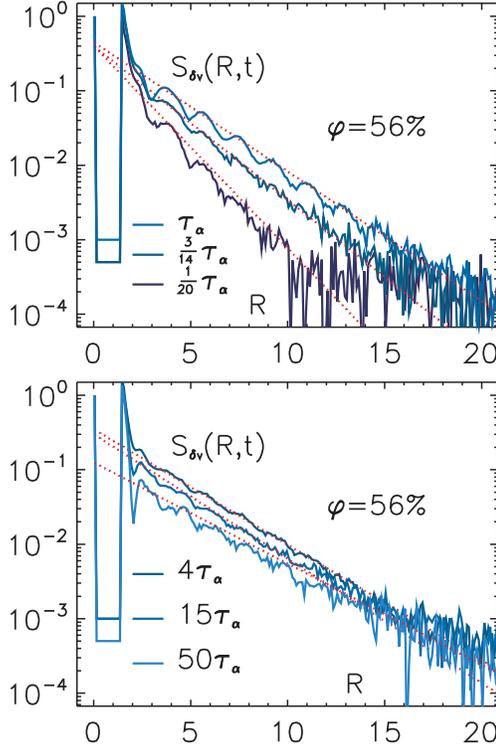
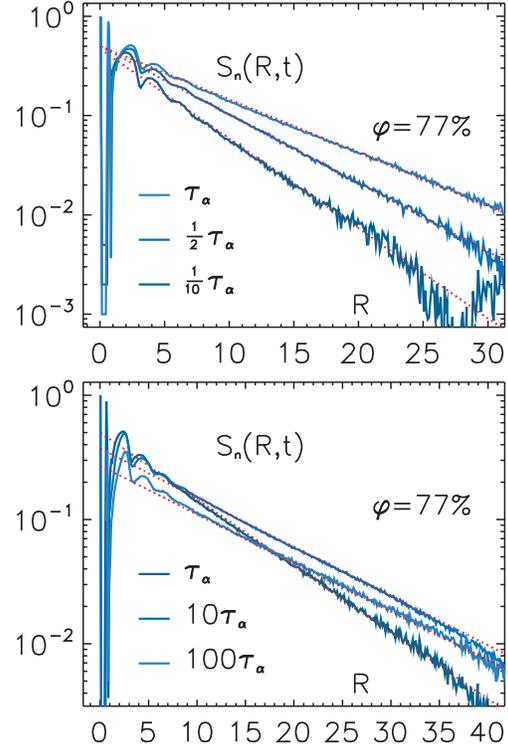Fig. 11: Spatial correlation $S_{\delta v}(R,t)$ at $\varphi_{3d} = 56\%$.

Fig. 12: Spatial correlation $S_{\mathbf{n}}(R,t)$ at $\varphi_{2d} = 77\%$.

Table 2:

φ_{2d}	0.73	0.75	0.77	0.78
$\#\tau_\alpha$	2000	5000	5000	500
N	8756	8960	9201	9320

φ_{3d}	0.53	0.56
$\#\tau_\alpha$	1500	750
N	15422	16307

we see in Fig. 12, $S_{\mathbf{n}}(R,t)$ is quite similar to $S_{\delta v}(R,t)$, i.e. we find an overall exponential decay of correlations with distance R. Its characteristic length $\xi_{\mathbf{n}}(t)$, however, is much larger than the previous $\xi_{\delta v}(t)$ (see below). Again, the situation is quite the same in three dimensions (Fig. 13), i.e. $\xi_{\mathbf{n}}$ exeeds $\xi_{\delta v}$ for $\varphi_{3d} = 0.56$. A remarkable difference to the 2d case are the extreme oscillations of $S_{\mathbf{n}}(R,t)$ for $t = \frac{1}{75}\tau_\alpha$. This is not understood yet, but could be due to the lower polydispersity in the three-dimensional system causing locally less amorphous packings. The vectorial correlation $S_{\mathbf{v}}(R,t)$ is also shown in Fig. 13, where it seems that the amplitude $A_{\mathbf{v}}(t)$ is a constant for all time scales $t > \tau_\alpha$.

Figure 14 summarizes the data for $\xi_X(t)$, $X_i = \delta v_i$. First of all, we notice an increase of correlation lengths with density. For a 3d Lennard-Jones system [1] and polymers [2], this has already been demonstrated for the special choice of time scale $t \approx \tau_\alpha$. But for longer times, even larger correlation lengths can be observed as shown in the figure. Interestingly, $\xi_X(t)$ is a monotonously increasing function, with a limiting value $\xi_X(\infty) \equiv \lim_{t \to \infty} \xi_X(t)$. For comparison, Fig. 14 shows the length scales for the directional correlation $\xi_{\mathbf{n}}(t)$ at $\varphi_{2d} = 0.77$ and $\varphi_{3d} = 0.56$.

Table 3 summarizes the data for $\xi_X(\infty)$, where the error due to fitting the exponential is less than ten percent. (The quantity R_{curl} will be explained below.) The statistical error due to finite time averages is small enough to be included therein. As we see, the length scale $\xi_{\delta v}(\infty)$ takes a snuggish rise, growing from 4.1 to 7.15 between $\varphi_{2d} = 0.73$ and 0.77. In contrast, $\xi_{\mathbf{n}}$ and $\xi_{\mathbf{v}}(\infty)$, starting from about the same initial value, end up at a value of more than twice $\xi_{\delta v}(\infty)$. The underlying physics of this very different behavior of mobility and directional correlations is unclear. As in the case of N_X^{coop}, the vectorial quantities $\mathbf{n}_i$ and $\mathbf{v}_i$ show a very simi-
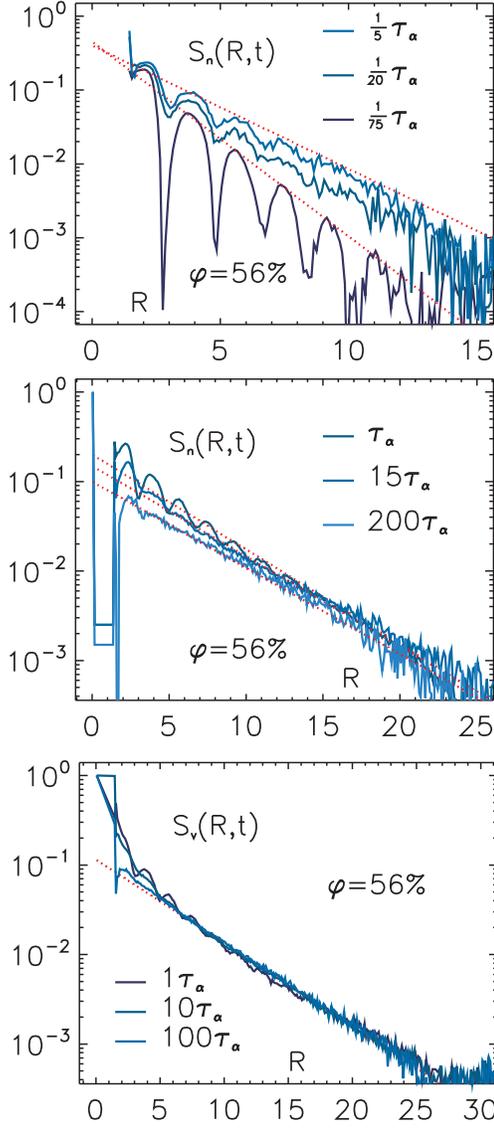
Fig. 13: Spatial correlation $S_{\mathbf{n}}(R;t)$ and $S_{\mathbf{v}}(R;t)$ at $\varphi_{3d} = 56\%$.

Table 3:

φ_{3d}	0.53	0.56
$\xi_{\delta v}(\infty)$	2.2	2.8
$\xi_{\mathbf{n}}(\infty)$	2.3	4.5
$\xi_{\mathbf{v}}(\infty)$	-	4.6

φ_{2d}	0.73	0.75	0.77	0.78
$\xi_{\delta v}(\infty)$	4.1	5.2	6.0	7.2
$\xi_{\mathbf{n}}(\infty)$	3.7	5.4	11	16
$\xi_{\mathbf{v}}(\infty)$	4	-	10.5	16
$R_{\mathrm{curl}}(\infty)$	8	10	21	30

$$= \int_0^\infty \mathrm{d}R\, p(R) S_X(R),$$

where $p(R)$ is the average number of particles found at distance R from a particle at the origin. In a way, this is a trivial result because the sum over all spatial correlations should be the overall cooperativity. When the approximation $S_X(R) \approx A e^{-R/\xi}$ is valid and at homogeneous density, we find $N_X^{\mathrm{coop}}(t) \sim \xi_X(t)^3 A(t)$. The deviations from the exponential for small R can modify this argumentation, but are unlikely to totally change the picture.

Consequently, the results for $N_{\delta v}^{\mathrm{coop}}(t)$ and $\xi_{\delta v}$ are only compatible, if the strength of correlation $A_{\delta v}(t)$ will tend to zero for long times. We can observe the decrease of $A_{\delta v}(t)$ clearly in Fig. 9 ($\varphi = 0.73$), but it is harder to see at higher densities because of the limited time window. For $X_i = \mathbf{v}_i$, in contrast, we need a limiting value of $A_{\mathbf{v}}$ greater than zero, if $S_{\mathbf{v}}(R,t)$ is to be compatible with $N_{\mathbf{v}}^{\mathrm{coop}}(t)$ for $t \to \infty$. Figure 13 proves this to be the case because $A_{\mathbf{v}}(t)$ is constant for $t > \tau_\alpha$.

Let us finally return to the detailed picture of Fig. 8. It suggests, that spatial correlations *along* the direction of motion will be very different from them *perpendicular* to it. We can test this by restricting the summation in Equ.(6) to certain angles ψ between the motion of particle i and the connection vector $\mathbf{r}_j - \mathbf{r}_i$. For example, the condition $\psi \in [\frac{\pi}{3}, \frac{2\pi}{3}]$ chooses only particles j that are *collateral* to particle i with respect to its motion $\mathbf{v}_i$. To select *in direction* of motion, we demand $\psi \in [0, \frac{\pi}{20}] \cup [\frac{19}{20}\pi, \pi]$, for example. The restricted sum is then carried out to obtain $S_{\mathbf{n}}^\perp(R,t)$ or $S_{\mathbf{n}}^{||}(R,t)$, see Fig. 15. Because of the backflow, we expect $S_{\mathbf{n}}^{||}(R,t)$ to become negative for large $R > 20$. This can be observed in the figure. In contrast, $S_{\mathbf{n}}^{||}(R,t)$ approaches zero

lar behavior of their inter-particle correlators.

So we can say, that the overall cooperativity is determined by both its length scale $\xi_X(t)$ and its strength, or amplitude, $A(t)$. Eqns. (2) and (7) show that

$$N_X^{\mathrm{coop}} \equiv 1 + \frac{\sum_{i \neq j} \langle X_i X_j \rangle}{\sum \langle X_i^2 \rangle}$$

$$= \frac{1}{\sum \langle X_i^2 \rangle} \sum_{ij} \langle X_i X_j \rangle$$

$$= \frac{1}{\langle X^2(0) \rangle} \int_0^\infty \mathrm{d}R\, p(R) \langle X(0) X(R) \rangle$$
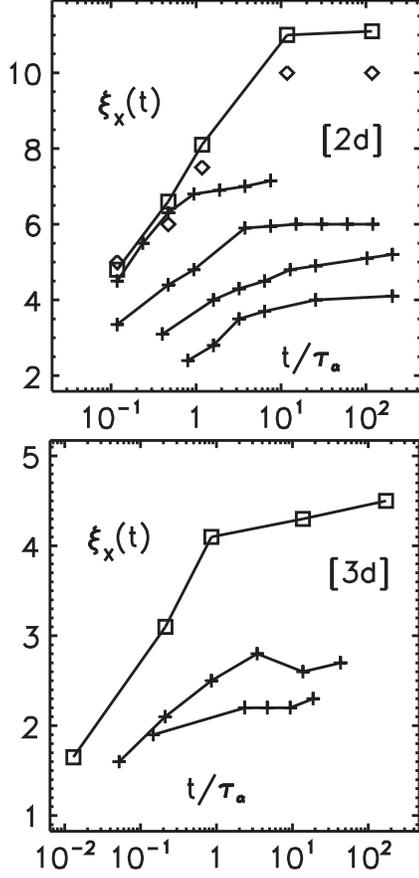
Fig. 14: [2d]: The dynamical length scales $\xi_{\delta v}(t)$ at packing fractions $\varphi_{2d} = 73\%$, 75%, 77% and 78%, from botton to top (+). For comparison: $\xi_{\mathbf{n}}(t)$ ($\square$) and $\frac{1}{2}R_{\mathrm{curl}}(t)$ ($\diamond$) at $\varphi_{2d} = 77\%$. [3d]: Again $\xi_{\delta v}(t)$ for the 3d densities $\varphi_{3d} = 53\%$ and 56% (+) and $\xi_{\mathbf{n}}(t)$ at $\varphi_{3d} = 56\%$ ($\square$). Errors due to fitting are estimated to be less than ten percent.

Fig. 15: Spatial correlation $S_{\mathbf{n}}(R,t)$ at $\varphi_{2d} = 77\%$, $t = 10\tau_\alpha$ and $\varphi_{3d} = 56\%$, $t = \tau_\alpha$, calculated dependent on the angle $\psi = (\mathbf{v}_i, \mathbf{r}_j - \mathbf{r}_j)$. Parallel ($\parallel$) means $\psi \in [0, \frac{\pi}{20}] \cup [\frac{19}{20}\pi, \pi]$, perpendicular ($\perp$) means $\psi \in [\frac{\pi}{3}, \frac{2\pi}{3}]$, and bulk stands for $\psi \in [0, \pi]$. In the perpendicular case, $S_{\mathbf{n}}(R,t)$ becomes zero at $R \approx R_{\mathrm{curl}}$ and is negative for larger distances, so that it is necessary to plot its absolute value.

fo $R \to \infty$. We notice the difference of length scales $\xi_{\mathbf{n}}^\perp$ and $\xi_{\mathbf{n}}^\parallel$, which is summarized in Table 4. The estimated error of these length scales

Table 4:

φ	0.56	0.77
$\xi_{\mathbf{n}}^\perp(\infty)$	2.7	7.5
$\xi_{\mathbf{n}}^\parallel(\infty)$	4.4	15

is less than 20 percent, but the exact values are not of interest here. Instead, the notion of a very different behavior of particles parallel and perpendicular to the motion of the central one is justified for three as well as for two-dimensional systems.
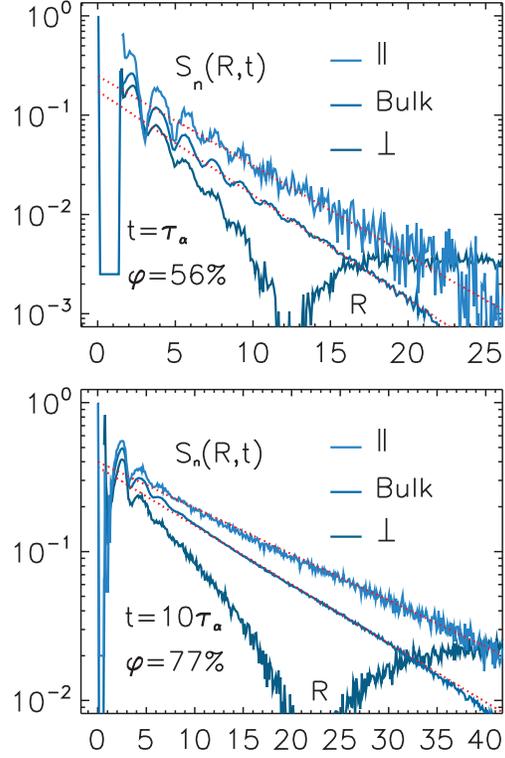
The time dependence $\xi_X(t)$, if at first sight surprising, can be understood quite pictorially. Without any further information, the probability for the motion of some tagged particle i is equal in every direction. However, if we know that, in the meanwhile, one or more of its next neighbors perform some specified displacements, this will influence the probability of movement of the tagged particle. More distant neighbors will do this as well, but the information about their motions has to be 'submitted' to particle i via nearer neighbors. It is not hard to imagine that the information spread can only take place with a finite velocity. Thus, short-time motions will be accompanied by a reaction of few neighbors, while long-lasting displacements will involve many of them. The monotonously growing length scale of dynamic correlations is the natural consequence.

In the limit $t \to \infty$, we can argue as in the case of N_X^{coop}: For long waiting times, the displacements $\mathbf{u}_i = \mathbf{r}_i(\frac{t}{2}) - \mathbf{r}_i(0)$ and $\mathbf{w}_i = \mathbf{r}_i(t) - \mathbf{r}_i(\frac{t}{2})$ become independent to a good approximation. Thus, correlations on time scale t can be expressed through $\mathbf{u}_i$ and $\mathbf{w}_i$, using $\mathbf{v}_i = \mathbf{u}_i + \mathbf{w}_i$:

$$\langle \mathbf{v}(0)\mathbf{v}(R) \rangle \approx \langle \mathbf{u}(0)\mathbf{u}(R) \rangle' + \langle \mathbf{w}(0)\mathbf{w}(R) \rangle'' .$$

This results in

$$S_{\mathbf{v}}(R,t) \approx \frac{1}{2} S_{\mathbf{v}}' \left(R, \frac{t}{2} \right) + \frac{1}{2} S_{\mathbf{v}}'' \left(R, \frac{t}{2} \right) .$$

The primed and double primed versions of $S_{\mathbf{v}}(R,t)$, respectively, denote measuring the distances R at the end or at the beginning of the time interval $[0,t]$. On the other hand, $S_{\mathbf{v}}(R,t)$ is defined by using the interparticle distance R in the middle of this interval. However, the definitions $S_{\mathbf{v}}(R,t)$, $S_{\mathbf{v}}'(R,t)$ and $S_{\mathbf{v}}''(R,t)$ produced the same results in our simulations, which is not shown here. Thus, in the long-time limit, the spatial correlations of the vectorial displacements $X_i = \mathbf{v}_i$ become time-independent, i.e.

$$S_{\mathbf{v}}(R,t) \approx S_{\mathbf{v}} \left(R, \frac{t}{2} \right) .$$

The phenomenon of a growing dynamical length scale is exibited by much simpler systems, like a one-dimensional (closed) chain of N diffusive particles which are connected by harmonic springs, as described by the Langevin equation

$$\dot{x}_n = -k(2x_n - x_{n-1} - x_{n+1}) + \eta_n,$$

where the η_n are independent white noises. Let us assume that N is a large number, say $N > 1000$. The analytic solution of this many-particle problem is possible with the help of discrete Fourier transform. This enables us to calculate the displacement-displacement correlation, but this is not shown here. In this simple model, the length of correlation increases with time, too. In contrast to our simulations, $\xi_{\mathbf{v}}(t)$ grows until it has reached the system size. Only from this time on center-of-mass diffusion prevails, for which correlations among different particles are no longer relevant. Stated differently, apart from finite size effects the chain model possesses $\xi_{\mathbf{v}}(\infty) = \infty$. In turn, we see the reason for a finite value of $\xi_X(\infty)$ in our HS systems:

"Particles simply can go out of each other's way".

In other words, a particle that travels a long distance does not have to pull the whole system

with it because rearrangements are possible. On average, this results in the back-flow behavior of Fig. 8. We are therefore tempted to relate the length scales $\xi_X(\infty)$ to an inherent length of the back-flow pattern for long times. From Fig. 8, we see that the distance $R_{\text{curl}}(t)$ from the vortices to the central particle is the only sensible choice. Table 3 shows the limiting values $R_{\text{curl}}(\infty)$ for the 2d systems under investigation. Interestingly, $R_{\text{curl}}(\infty)$ is twice the correlation length $\xi_{\mathbf{v}}(\infty)$ or $\xi_{\mathbf{n}}$. For $\xi_{\delta v}(\infty)$, no such relation seems to exist.

4   Discussion

We presented detailed information about displacement correlations, which turned out to be of the same nature for two-dimensional discs and three-dimensional hard spheres.

Using the quantities $X_i = \delta v_i$, $\mathbf{n}_i$ and $\mathbf{v}_i$ as input for $N_X^{\text{coop}}(t)$ and $S_X(R,t)$, we were able to measure the total reduction of degrees of freedom and the spatial extent of correlations, respectively. The data of N_X^{coop} is found to agree for these three choices of X_i, supporting the notion of a reduced dimensionality of motion in high-dimensional configuration space. The length scale of correlations, however, turns out to increase much faster with density for $X_i = \mathbf{n}_i$ and $\mathbf{v}_i$ than for $X_i = \delta v_i$. An explanation for this is lacking at the moment. Finally, we demonstrated, that for 2d as well as for 3d systems, an angle-resolved calculation of correlations is appropriate, yielding much larger length scales *in the direction of motion* than *perpendicular* to it.

The important question arises how the dynamical length scales $\xi_X(\infty)$ are connected to static correlations. Naive attempts, using, e.g. spatial density correlations, have not revealed any significant connection. What makes things more complicated is $\xi_X(t)$'s dependence on the definition of X_i. On the other hand, $N_X^{\text{coop}}(t)$ and $S_X(R;t)$ are strongly averaged quantities, obtained by including many different dynamical situations. Thus, we should not hope to get too specific information from them. A deeper understanding of cooperative effects will only become possible by a more detailed, less averaged treatment. In any way, the relation of structure to dynamics is the central problem to be solved. The present work may help to formulate the relevant questions somewhat clearer.

der Chemischen Industrie.

References

[1] P. H. Poole, C. Donati, and S. C. Glotzer. *Physica A*, 261(1-2):51–59, Dec 1998.

[2] C. Bennemann, C. Donati, J. Baschnagel, and S. C. Glotzer. *Nature*, 399(6733):246–249, May 1999.

[3] C. Donati, S. C. Glotzer, P. H. Poole, W. Kob, and S. J. Plimpton. *Phys. Rev. E*, 60(3):3107–3119, Sep 1999.

[4] R. Yamamoto and A. Onuki. *Phys. Rev. E*, 58(3):3515–3529, Sep 1998.

[5] U. Tracht, M. Wilhelm, A. Heuer, H. Feng, K. Schmidt-Rohr, and H. W. Spiess. *Phys. Rev. Lett.*, 81(13):2727–2730, Sep 1998.

[6] U. Tracht, H. Wilhelm, A. Heuer, and H. W. Spiess. *J. Magn. Reson.*, 140(2):460–470, Oct 1999.

[7] C. Donati, S. Franz, G. Parisi, and S. C. Glotzer. *cond-mat/9905433*, v3, Jun 1999.

[8] C. Donati, S. C. Glotzer, and P. H. Poole. *Phys. Rev. Lett.*, 82(25):5064–5067, Jun 1999.

[9] S. C. Glotzer, V. N. Novikov, and T. B. Schroder. *cond-mat/9905433*, v3, Jun 1999.

[10] P. Maass, M. Meyer, and A. Bunde. *Phys. Rev. B-Condens Matter*, 51(13):8164–8177, Apr 1995.

[11] I. Moriguchi, K. Kawasaki, and T. Kawakatsu. *J. Phys. II*, 3(8):1179–1184, Aug 1993.

[12] T. Gleim, W. Kob, and K. Binder. *Phys. Rev. Lett.*, 81(20):4404–4407, Nov 1998.

[13] W. Götze and L. Sjogren. *Rep. Prog. Phys.*, 55(3):241–376, Mar 1992.

[14] B. Doliwa and A. Heuer. *Phys. Rev. Lett.*, 80(22):4915–4918, Jun 1998.

[15] B. Doliwa and A. Heuer. *J. Phys.-Condes. Matter*, 11(10A):A277–A283, Mar 1999.

[16] F. Kolbe. *Diploma Thesis, University of Konstanz*, Dec 1998.

[17] D. N. Perera and P. Harrowell. *Phys. Rev. E*, 59(5):5721–5743, May 1999.

[18] B. J. Alder and T. E. Wainwright. *Phys. Rev. A*, 1(18), 1970.

[19] G. Johnson, A. I. Mel'cuk, H. Gould, W. Klein, and R. D. Mountain. *Phys. Rev. E*, 57(5):5707–5718, May 1998.